John von Neumann Institute for Computing

The Fine-Scale Structure of Turbulence

J. Schumacher, M. S. Emran, B. Eckhardt

published in

NIC Symposium 2008,
G. Münster, D. Wolf, M. Kremer (Editors),
John von Neumann Institute for Computing, Jülich,
NIC Series, Vol. **39**, ISBN 978-3-9810843-5-1, pp. 341-348, 2008.

http://www.fz-juelich.de/nic-series/volume39

The Fine-Scale Structure of Turbulence

Jörg Schumacher[1]**, Mohammad S. Emran**[1] **and Bruno Eckhardt**[2]

[1] Department of Mechanical Engineering, Technische Universität Ilmenau, 98684 Ilmenau

[2] Fachbereich Physik, Philipps-Universität Marburg, 35032 Marburg
E-mail: Joerg.Schumacher@tu-ilmenau.de

The fine-scale structure of turbulence is studied in three systems: fluid turbulence, scalar mixing, and turbulent convection. It is always characterized by large fluctuations of the corresponding field gradients which are probed by dissipation rate fields. We discuss the statistics of these quantities and the associated characteristic scales of the most intense dissipation fluctuations.

1 Introduction

Turbulence remains an outstanding fundamental problem of classical physics because of its disordered, unsteady and nonlinear dynamics which covers a wide range of scales in length and time. These variations also give rise to large fluctuations of steep gradients, which appear preferentially at the smallest scales of the flow. The amplitudes of the gradients do not follow a Gaussian distribution, and extremal values frequently exceed the mean values by orders of magnitude. This phenomenon is known as *small-scale intermittency*[1–3]. It is believed that these intense fine-scale fluctuations are intimately connected with the nonlinear cascade-like transfer of energy through the hierarchy of turbulent structures. In order to arrive at a better understanding of turbulence as a whole, we here present results from a high resolution study of the intermittent dynamics at the small-scale end of the cascade range. Such analysis is also important for the mixing in reacting and non-reacting flows, especially when a significant fraction of stirring of the concentration field takes place at the small scales of the flow. This is the case when the scalar diffusivity is small in comparison to the viscosity of the fluid.

In the absence of an analytical theory, direct numerical simulations (DNS) of the underlying fluid transport equations are the most promising approach to uncover these statistical and structural properties of turbulence, where the steepest gradients and their statistics can be resolved. Experiments cannot yet reach the finest scale filaments, despite significant progress in measurement techniques.

A fundamental quantity which probes the gradient magnitudes and displays the small-scale intermittency is the dissipation rate. In the following, we study the statistics and geometry of dissipation rate fields in three different turbulent flows: fluid turbulence, passive scalar mixing and turbulent Rayleigh-Bénard convection. For fluid turbulence, we take the energy dissipation rate of the velocity field $\mathbf{u}(\mathbf{x},t)$, given by

$$\epsilon(\mathbf{x},t) = \frac{\nu}{2}(\partial_i u_j + \partial_j u_i)^2 \,, \tag{1}$$

where ν is the kinematic viscosity of the fluid and $i,j = x,y,z$. Our second example is the *passively* advected concentration field $\theta(\mathbf{x},t)$, with dissipation rate

$$\epsilon_\theta(\mathbf{x},t) = \kappa(\partial_i \theta)^2 \,, \tag{2}$$

where κ is the diffusivity. Our final example is thermal convection, where the temperature field $T(\mathbf{x}, t)$ represents an *active* scalar field that can react back onto the flow by buoyancy. The corresponding thermal dissipation rate is given by

$$\epsilon_T(\mathbf{x}, t) = \kappa(\partial_i T)^2 \,. \tag{3}$$

with κ the thermal diffusion constant.

As we will see, extremal values of the dissipation field occur preferentially in form of thin sheets. A characteristic scale which is associated with the dissipation maxima is therefore the cross-section thickness scale of the sheets. The fluctuating nature of the dissipation generates a whole range of these scales, thus replacing the mean dissipation scale usually considered by a distribution of dissipation scales.

2 Fluid Turbulence

The continuity and Navier-Stokes equations for an incompressible fluid are given by

$$\nabla \cdot \mathbf{u} = 0 \,, \tag{4}$$

$$\frac{\partial \mathbf{u}}{\partial t} + (\mathbf{u} \cdot \nabla)\mathbf{u} = -\nabla p + \nu \nabla^2 \mathbf{u} + \mathbf{f} \,. \tag{5}$$

Here, $\mathbf{u}$ is the three-dimensional turbulent velocity field, $\mathbf{f}$ is a forcing field which sustains the statistical stationarity of turbulence and p is the (kinematic) pressure field. The dimensionless parameter that characterizes the flow is the Reynolds number based on the velocity fluctuations,

$$Re = \frac{\langle u^2 \rangle^{1/2} L}{\nu} \,. \tag{6}$$

The equations are solved by a pseudospectral method in a periodic box of side length $L = 2\pi$. More details are given in Schumacher *et al.*[4]. In contrast to many other large scale simulations with a similar number of nodes, the highest Reynolds numbers studied here are moderate: since we are interested in the small scales we cannot sacrifice small scale resolution in order to achieve high Reynolds numbers, as often done (some of the problems with such an approach are illustrated using shell models in Ref. 5). But the simulations do set a record in that they reach down to the smallest scales ever resolved.

Kolmogorov refined his classical hypothesis by incorporating the fluctuating nature of the dissipation rate field and predicted a log-normal statistics for ϵ (see Refs. 1 and 2). This is the point of reference for studies of small-scale intermittency in turbulence. Fig. 1 shows a snapshot of the dissipation field. The intermittent nature of the quantity is reflected in the few localized very-large amplitude regions which are embedded in an ambient and less strongly varying dissipation background. The extreme events will be found in the tails of the probability density function of the dissipation field. In Fig. 2, we show the PDFs of the dissipation field obtained from our high-resolution simulations for different Reynolds numbers. We see that systematic deviations of the statistics from log-normality appear in the far tails, i.e. for extremely small and large amplitudes. In other words, the log-normal model will differ for higher-order moments of the dissipation rate field. The dependence of these moments on the Reynolds number Re was derived recently by Yakhot and Sreenivasan[6]. The approach starts from the Navier-Stokes equations and gives a relation between moments of the energy dissipation and the scaling of the structure functions in the inertial range:

$$\langle \epsilon^n \rangle \sim Re^{n+\frac{\zeta_{4n}}{\zeta_{4n}-\zeta_{4n+1}-1}} . \tag{7}$$

where ζ_n are the scaling exponents of the velocity structure function in the inertial cascade range of turbulence. Relation (7) connects the physics at small scales –the scales where the dissipation field fluctuates– with the velocity statistics in the inertial range. Such relations are also known as bridge relations. The strong resolution requirements are reflected in the large order of ζ_n. A dissipation moment of order 4 is not converged before the analytic range of the velocity structure function of order 16 is resolved! This justifies the resolution and the numerical efforts taken here. Table 1 compares our simulation results with the classical theory and Ref. 6. The recent approach agrees quite well with the simulation results while the log-normal model deviates as already seen in Fig. 2. A further consequence of Ref. 6 is that a whole range of characteristic dissipation scales exists instead of one mean scale as in the classical theory of turbulence[7].

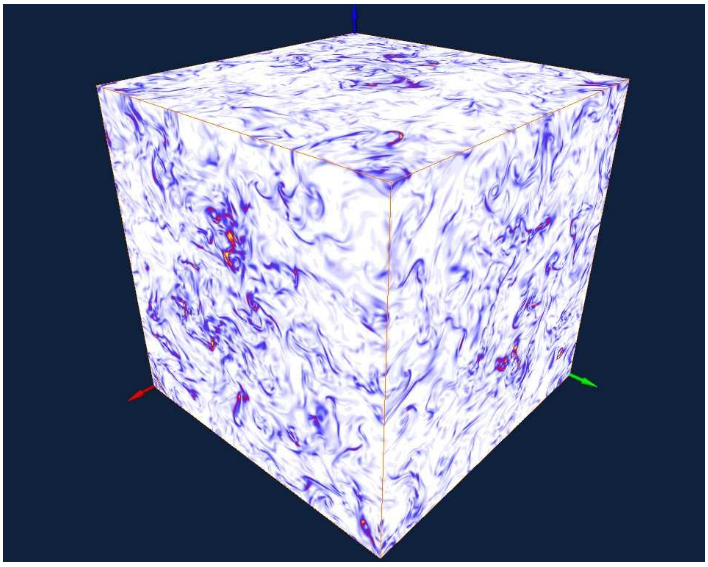

Figure 1. Contour plots of the energy dissipation rate field ϵ taken at the sideplanes of the cube. Data are from a simulation with a resolution of $N^3 = 2048^3$ grid points for a volume $V = (2\pi)^3$.

3 Passive Scalar Turbulence

In passive scalar turbulence, the concentration field $\theta(\mathbf{x}, t)$ is advected by a turbulent flow according to the advection-diffusion equation,

$$\frac{\partial \theta}{\partial t} + (\mathbf{u} \cdot \nabla)\theta = \kappa \nabla^2 \theta + f_\theta . \tag{8}$$

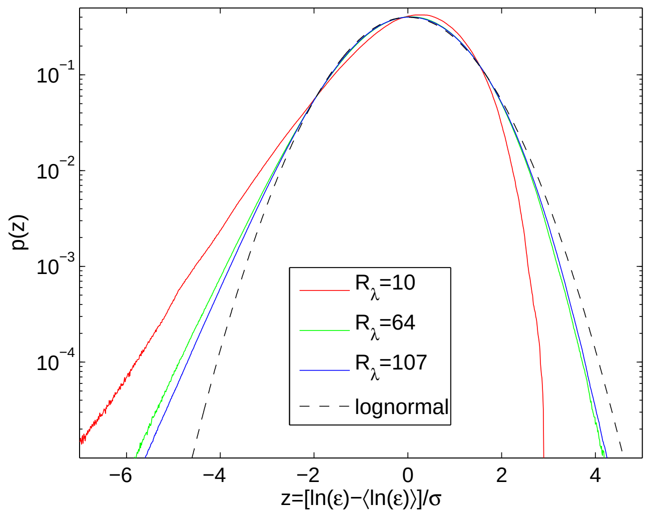

Figure 2. Probability density functions of the energy dissipation rate field at different Taylor microscale Reynolds numbers. The data are compared to the log-normal distribution which was suggested by Kolmogorov and Oboukhov in 1962. Systematic deviations from this small-scale intermittency model can be seen in particular for the rare low- and large-amplitude events which are found in the tails of the distribution.

	Theory (Yakhot)	Simulation	Kolmogorov (1962)
d_2	0.157	0.152	0.173
d_3	0.489	0.476 ± 0.009	0.465
d_4	0.944	0.978 ± 0.034	0.844

Table 1. Comparison of scaling exponents for energy dissipation rate moments of order 2, 3 and 4 with theories. In the simulations the moments and their dependence on the Reynolds number can be directly measured. Exponents are given by $d_n = n + \zeta_{4n}/(\zeta_{4n} - \zeta_{4n+1} - 1)$ in Ref. 6. and $d_n = 3(n - \zeta_{3n})/4$ in Refs. 1 and 2.

Here, f_θ is a force that sustains statistically stationary scalar fluctuations. Boundary conditions, numerical scheme and geometry are the same as for the pure fluid case. The dimensionless parameter of interest is the Schmidt number. It is given by

$$Sc = \frac{\nu}{\kappa} \,. \tag{9}$$

For $Sc > 1$, a significant fraction of the scalar is advected by the small-scale velocity field, very similar to chaotic advection[8,9]. The resulting scalar dissipation field is shown in Fig. 3. The local maxima of the dissipation field are curved sheets which result in the red coloured filaments for a plane cut as in the left panel[10]. The local cross-section thickness of these filaments was detected by a fast multiscale image segmentation algorithm[5]. Its application to the simulation data is demonstrated in the right panel. The local thickness is given then by the second principal component value which is calculated for each of the differently coloured subfilaments. The distribution of the scales l_d is shown in Fig. 4 for different Reynolds and Schmidt numbers. Rescaling of the distributions by the corresponding mean dissipation scale (Kolmogorov scale η for the Reynolds number dependence and the Batchelor scale $\eta_B = \eta/\sqrt{Sc}$ for the Schmidt number dependence at fixed Reynolds number) results in a collapse of the data for different parameters. As in the case of fluid turbulence, we can find a whole range of *local* dissipation scales which are here directly determined from the largest amplitudes of the dissipation field.

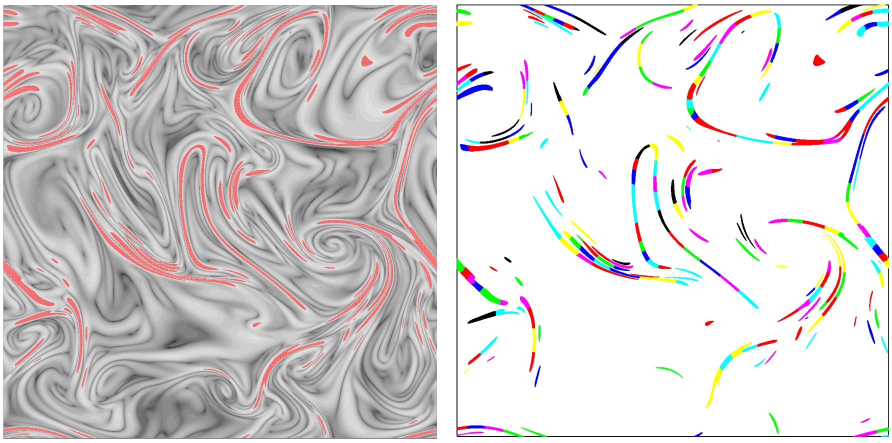

Figure 3. Left: Contour plot of a two-dimensional slice cut through the instantaneous three-dimensional scalar dissipation rate field ϵ_θ. Local maxima are replotted in red. The Schmidt number is 32 and the Taylor microscale Reynolds number is 24. The mean Batchelor scale is resolved with 2 grid cells in the simulation. Right: Reconstruction of the red coloured filaments as shown to the left by means of the fast multiscale clustering algorithm. Long filaments are composed of several subfilaments that are coloured differently.

4 Turbulent Rayleigh-Bénard Convection

In our final example we study turbulent convection, and take the influences from confining boundaries into account. We describe the temperature field within the Boussinesq approximation, and assume that the mass density of the fluid varies linearly with temperature. Temperature fluctuations drive the fluid motion by a buoyancy term that has to be substituted in the Navier-Stokes equations (5). It is given by

$$\mathbf{f}(\mathbf{x},t) = g\alpha T(\mathbf{x},t)\mathbf{e}_z \,. \tag{10}$$

α is the thermal expansion coefficient and g the gravity acceleration. The equation for the temperature field is the same as in the passive scalar case. It is given by

$$\frac{\partial T}{\partial t} + (\mathbf{u}\cdot\nabla)T = \kappa\nabla^2 T \,. \tag{11}$$

The Boussinesq equations are solved in a cylindrical cell with solid walls by a finite difference scheme. No-slip boundary conditions hold for the velocity field. The hot bottom

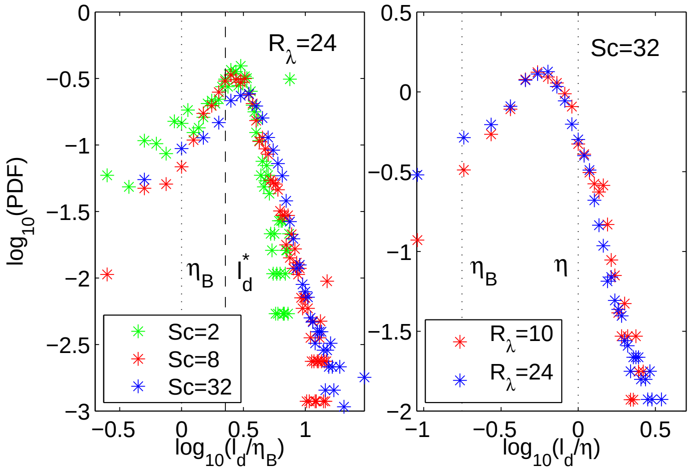

Figure 4. Distribution of the local cross section thickness l_d of the scalar dissipation rate filaments as highlighted in Fig. 3. Left panel: PDF of local dissipation scales for three different Schmidt numbers at a fixed Reynolds number. The dashed line corresponds with the theoretical value of the most probable thickness scale. Right panel: PDF of the thickness scales for two different Reynolds numbers at a fixed Schmidt number.

plate and the cold top plate are held at fixed temperatures. The side walls are adiabatic. The dimensionless parameters are the Prandtl number Pr (equivalent to Sc), the Rayleigh number Ra which measures the magnitude of the temperature drop between top and bottom plate in z direction and the aspect ratio Γ which relates diameter D and height H

$$Pr = \frac{\nu}{\kappa}\,, \qquad Ra = \frac{\alpha g H^3 \Delta T}{\nu\kappa}\,, \qquad \Gamma = \frac{D}{H}\,. \tag{12}$$

Fig. 5 shows instantaneous snapshots of the total thermal dissipation rate ϵ_T (bottom) and the corresponding temperature T (top). A typical feature of turbulent convection are so-called *thermal plumes* which consist of hot blobs detaching from the boundary layer and rising into the cell. They are connected with large local thermal dissipation rate amplitudes which give the main contribution to the turbulent heat transport through the convection cell.

The temperature field is decomposed into a z-dependent mean profile $\langle T\rangle_A(z)$ and the fluctuations about the mean $\theta(\mathbf{x},t)$. Consequently, the thermal dissipation rate can be decomposed into two contributions,

$$\langle\epsilon_T\rangle_A(z) = \epsilon_{\langle T\rangle}(z) + \langle\epsilon_\theta\rangle_A(z)\,, \tag{13}$$

where $\langle\cdot\rangle_A$ is a time-plane average at fixed $z \in [0,H]$. Fig. 6 shows the vertical profiles of the three different terms in (13). It can be seen that the dominant part of the thermal dissipation close to the plates comes from the mean profile term. This suggests that the plumes affect the cell to a certain height only, an open question of present research on the subject. Towards the centre of the cell the total magnitude of the dissipation drops and is mainly due to the thermal fluctuations. Our present studies indicate that the statistical properties of the thermal dissipation rate field in the centre of the cell are very similar to

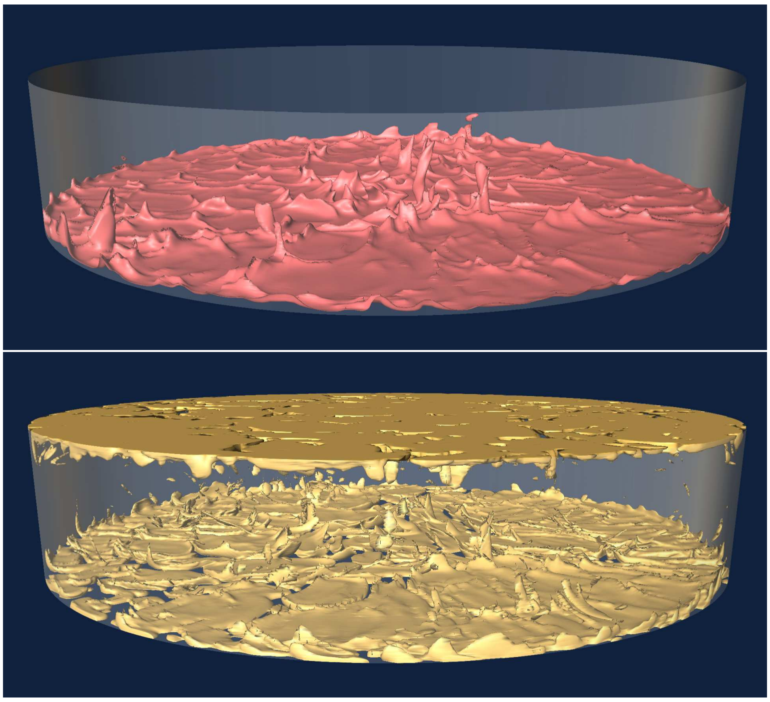

Figure 5. Snapshots of the temperature field T (top) and the corresponding thermal dissipation rate field ϵ_T (bottom) for turbulent convection in a cell with aspect ratio $\Gamma = 5$ at a Rayleigh number $Ra = 10^7$. The temperature level $T = 0.75T_{bottom}$ is shown. The isolevel of the thermal dissipation rate field is 0.02.

those of the passive scalar dissipation rate[9]. In both cases we find again deviations of the PDF from log-normality as shown for the velocity field in Fig. 2. The detailed study of the statistics of the thermal dissipation rate in the boundary layers is currently in progress.

Acknowledgments

We would like to thank W. J. A. Dahm, P. E. Hamlington, C. R. Doering, K. R. Sreenivasan, R. Verzicco and V. Yakhot for fruitful discussions. The research is supported by the Deutsche Forschungsgemeinschaft, by the German Academic Exchange Service (DAAD) and the DEISA consortium. We would like to thank the John von Neumann Institute for Computing for the steady support of our research. JS thanks especially M. Boltes, S. Habbinga, M.-A. Hermanns, M. Rambadt and H. Zilken for their support during the phase of the DEISA project "eta2006" and M. Pütz (IBM Deutschland) for getting started at the Blue Gene/L JUBL.

References

1. A. N. Kolmogorov, *A refinement of previous hypotheses concerning the local structure of turbulence in a viscous incompressible fluid at high Reynolds number*, J. Fluid Mech. **13**, 82-85, 1962.

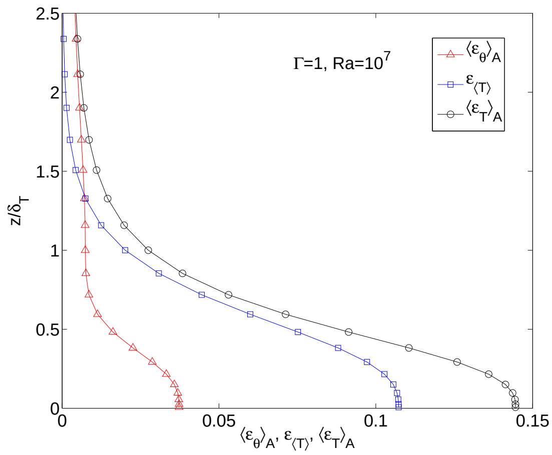

Figure 6. Vertical height dependence of the two different contributions to the total thermal dissipation rate ϵ_T as given by (13). Data are for a Rayleigh number $Ra = 10^7$ and an aspect ratio $\Gamma = 5$. The numerical grid is $N_\phi \times N_r \times N_z = 361 \times 257 \times 128$.

2. A. M. Oboukhov, *Some specific features of atmospheric turbulence*, J. Fluid Mech. **13**, 77-81, 1962.
3. K. R. Sreenivasan and R. A. Antonia, *The phenomenology of small-scale turbulence*, Annu. Rev. Fluid Mech. **29**, 435-472, 1997.
4. J. Schumacher, K. R. Sreenivasan and V. Yakhot, *Asymptotic scaling exponents from low-Reynolds number flows*, New J. Phys. **9**, 89, 2007.
5. J. C. Bowman, C. R. Doering, B. Eckhardt, J. Davoudi, M. Roberts and J. Schumacher, *Links between dissipation, intermittency, and helicity in the GOY model revisited*, Physica D **218**, 1-10, 2007.
6. V. Yakhot and K. R. Sreenivasan, *Towards a dynamical theory of multifractals in turbulence*, Physica A **343**, 147-155, 2004.
7. J. Schumacher, *Sub-Kolmogorov-scale fluctuations in fluid turbulence*, Europhys. Lett. **80**, 54001, 2007.
8. J. Schumacher, K. R. Sreenivasan and P. K. Yeung, *Very fine structures in scalar mixing*, J. Fluid Mech. **531**, 113-129, 2005.
9. J. Schumacher and K. R. Sreenivasan, *Statistics and geometry of passive scalar fields in turbulence*, Phys. Fluids **17**, 125107, .
10. J. Schumacher, H. Zilken, B. Eckhardt and K. R. Sreenivasan, *Scalar dissipation fronts in high-Schmidt number mixing (Gallery of Nonlinear Images)*, Chaos **15**, 041105, 2005.
11. D. Kushnir, J. Schumacher and A. Brandt, *Geometry of intensive scalar dissipation events in turbulence*, Phys. Rev. Lett. **97**, 124502, 2006.